Solution and Gas-Phase Stability of DNA Junctions from Temperature-Controlled Electrospray Ionization and Surface-Induced Dissociation

Adam Pruška, Julian A Harrison, Anton Granzhan, Adrien Marchand, Renato Zenobi

Solution and Gas-Phase Stability of DNA Junctions from Temperature-Controlled Electrospray Ionization and Surface-Induced Dissociation

Adam Pruška[‡1], Julian A. Harrison[‡1], Anton Granzhan[2], Adrien Marchand[1], and Renato Zenobi[1*]

[1]Department of Chemistry and Applied Biosciences, ETH Zurich, CH-8093 Zurich, Switzerland

[2]CNRS UMR9187, Inserm U1196, Institut Curie, Paris Saclay University, F-91405 Orsay, France

[‡]These authors contributed equally

ABSTRACT: DNA three-way junction (TWJ) structures transiently form during key cellular processes such as transcription, replication, and DNA repair. Despite their significance, the thermodynamics of TWJs, including the influence of strand length, base pair composition, and ligand binding on TWJ stability and dissociation mechanisms are poorly understood. To address these questions, we interfaced temperature-controlled nanoelectrospray ionization (TC-nESI) with a cyclic ion mobility mass spectrometry (cIM-MS) instrument that was also equipped with a surface-induced dissociation (SID) stage. This novel combination allowed us to investigate the structural intermediates of three TWJ complexes and examine the effects of GC base pairs on their dissociation pathways. We found that two TWJ-specific ligands, 2,7-TrisNP and TrisPOB, leads to TWJ stabilization, revealed by an increase in the melting temperature (T_m) by 13 or 26 °C, respectively. To gain insights into conformational changes in the gas phase, we employed IMS and SID to analyze TWJs and their complexes with ligands. Analysis of IM arrival distributions suggested a single-step dissociation of TWJs and their intermediates for the three studied TWJ complexes. Upon ligand binding, a higher SID energy by 3 V (2,7-TrisNP) and 5 V (TrisPOB) was required to induce 50% dissociation of TWJ, compared to 38 V in the absence of ligands. Our results demonstrate the power of utilizing TC-ESI in combination with cIMS and SID for thermodynamic characterization of TWJ complexes and investigation of ligand binding. These techniques are essential for the TWJ design and development as drug targets, aptamers, and structural units for functional biomaterials.

Introduction

The specific structures adopted by nucleic acids play essential role in numerous cellular processes, including transcription, replication, and DNA repair.[1] These processes require specific secondary and higher-order tertiary structures of DNA, to fulfill their respective functions; therefore, they represent promising biomolecular targets. Many researchers have put considerable effort into characterizing these biomolecules as well as developing drugs that specifically target them. Most of this research has focused on hairpins,[2] G-quadruplexes,[3–7] i-motifs,[8,9] and multi-way junctions. However, DNA junctions have recently received increased attention for their potential in cancer therapeutics.[10–12] Also, nucleic acids and their complexes can serve as structural units for bottom-up fabrication and sensing devices.[13–19]

Three-way junctions (TWJ) are non-covalent complexes composed of three partially complementary strands.[20] As shown in the Figure 1A, the junction is situated between all composing strands and represents a recognition site for a variety of binding partners, including proteins,[21–23] small molecules,[24–26] and metal ions.[27] TWJs are of significant interest for developing new treatment approaches because ligand binding[28] can alter their thermodynamic stability, cellular persistence, structure and/or functions.[26,29–31] Novel therapeutic approaches targeting junctions aim to inflict severe genetic injuries to cause failure of the proliferation machinery in malignant cells,[32] or control cellular processes.[10,11] TWJ formation and stability is dependent on strand length, the presence of mismatches, and the self-duplex formation.

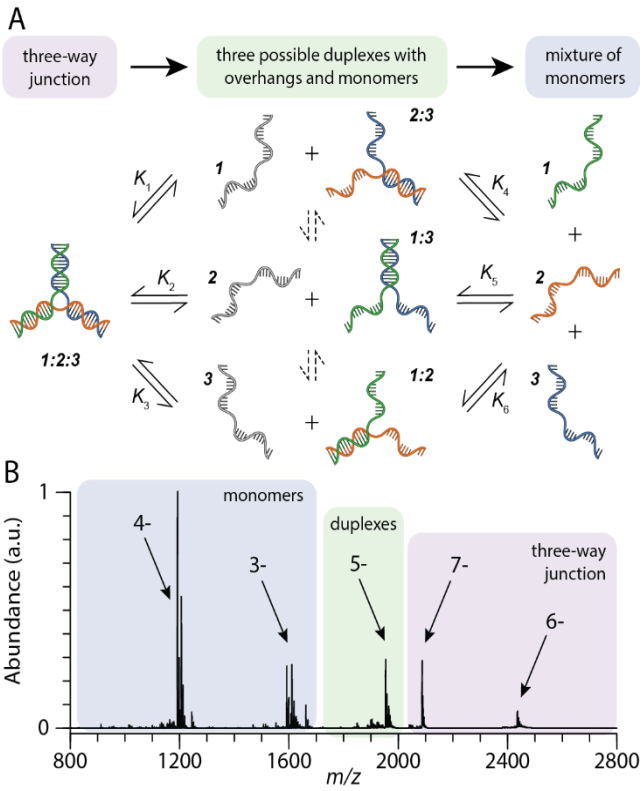

Figure 1: (A) The suggested scheme of three-way junction (TWJ) dissociation pathway with equilibrium constants. Initial structure of fully folded TWJ releases one of the strands with increasing temperature. Unfolded system contains only single strands at high temperature. (B) Mass spectrum of the 20 μM TWJ-3 (8 bps in each arm) averaged between 20 and 70 °C.

However, there is a paucity of data on unfolding and dissociation mechanisms of TWJs.[25,26,33–35] This is attributed to the structural complexity of TWJs, which arises from the dynamics of potential multiple conformational states. Furthermore, these structures likely adopt multi conformational states during formation/dissociation, as suggested in Figure 1A. The presence of these intermediate states means that methods such as nuclear magnetic resonance,[36] cryogenic electron microscopy,[37] and calorimetric analysis[34] are not well-suited for studying TWJs. A key limitation in the study of TWJs is the absence of tools that can provide insights into the thermodynamics and kinetics, specifically the identification of intermediates that take place during dissociation processes.

Native mass spectrometry (MS) is a powerful method that can be used for such investigations. Previous studies have demonstrated that it is possible to characterize unfolding and dissociation mechanisms and ligand binding to DNA structures by MS, since non-covalent interactions, responsible for DNA secondary structure formation, can be preserved in the gas phase.[38–40] However, it remains an open question whether solution and gas-phase stabilities correlate, despite the considerable effort researchers have put into understanding the gas and solution phase behavior of protein[41–45] and DNA complexes.[46–50]

One way of addressing this issue is by using temperature-controlled nanoelectrospray (TC-nESI), where the temperature of the spray solution is controlled, and temperature-induced changes are monitored by MS.[5,51–58] From this information, is it is possible to obtain thermodynamic information, and the nature and abundance of structural intermediates can be characterized. This type of analysis was exemplified in our previous work examining the thermodynamics of DNA G-quadruplex structures.[58,59] Other recently commercialized technologies, such as surface-induced dissociation (SID)[60] and cyclic ion mobility (cIMS)[61] have yet to be applied to such biomolecules. In this work, a combination of TC-nESI,[62] SID, cIMS, UV-melting, and circular dichroism (CD) spectroscopy were used to examine the dissociation mechanism of three TWJs (Table 1). We compared the effects of nucleotide composition, strand length, and TWJ-binding ligands on TWJ stability to study their thermodynamics in unprecedented detail.

Methods

Oligonucleotide Preparation

Oligonucleotides were designed to avoid mismatches and direct interaction of single strands between two or more domains.[63] All oligonucleotides were obtained in the form of reverse-phase purified, dried samples (Eurogentec). To

prevent undesired structural assemblies, the samples were dissolved in 100 µL of DNAse-free water (Fisher Bioreagents), heated to 80 °C for 1 minute, allowed to cool to room temperature, and stored in the freezer. Oligonucleotide concentrations were calculated from the Beer-Lambert law, based on the absorbance at 260 nm measured by a spectrophotometer (Genesys 10S, Thermo Fisher Scientific). The extinction coefficients of single-stranded sequences were calculated using an online tool available on molbiotools.com. Unless otherwise specified, a 20 mM oligonucleotide solution was prepared in 100 – 300 mM ammonium acetate solution (AmAc; for molecular biology, Sigma-Aldrich) at physiological pH (7.4). Mixtures of three oligonucleotides of 7 – 20 µM each (listed in the Table 1) were heated to 85 °C and incubated overnight at 4 °C to form the complex.

Photometric Measurements and Structural Simulation

Circular Dichroism: CD experiments were performed using a Chirascan CD spectrophotometer (Applied Photophysics, Leatherhead, U.K.) equipped with a sealed quartz cuvette (Hellma Analytics, Müllheim, Germany) with a light path length of 1 mm. Full wavelength scans of ellipticity absorption were recorded in the range of 210 to 320 nm using a spectral bandwidth 1 nm, a step resolution 1 nm, and a 5 s time per point.

UV-Vis: Absorption spectra were acquired using a Cary 60 UV-Vis spectrophotometer equipped with a temperature-controlled multicell holder (both Agilent Technologies, USA). Pristine solvent was used for background subtraction. UV-Vis melting experiments were carried out with a gradient of 0.2 °C/min.

'DINAMelt Server' structural simulations were conducted to detected structural mismatches such as bulges, hairpins and duplexes formation. The ion concentrations, crucial for valid comparison with the MS thermal denaturation experiments, were set to 20 µM (oligonucleotides), 100 mM (Na^+), and 0 mM (Mg^{2+}).

Table 1. DNA oligonucleotides forming three-way junctions used in this study.

Name		Sequence (5' to 3')	Avg. Mass (Da)
inter. standard		TTTTTT	1763.22
TWJ-1	TWJ-1.1	ATCCGCATGACATTCGCCGT	5410.58
	TWJ-1.2	ACGGCGAATGACCGAATCAG	6160.08
	TWJ-1.3	CTGATTCGGTTCATGCGGAT	6139.04
TWJ-2	TWJ-2.1	CGGAACGGCACTCG	4273.84
	TWJ-2.2	CGAGTGCAGCGTGG	4344.87
	TWJ-2.3	CCACGCTCGTTCCG	4175.76
TWJ-3	TWJ-3.1	ATAGAACTGTCACATC	4849.24
	TWJ-3.2	CCACCGCTAGTTCTAT	4792.18
	TWJ-3.3	GATGTGACAGCGGTGG	5002.31

Mass Spectrometry

Mass spectra were acquired in negative mode utilizing an ion-mobility (IMS) spectrometer hyphenated with a time-of-flight (TOF) MS (SELECT SERIES Cyclic IMS, Waters Corp.) equipped with both an electron capture dissociation (ECD) cell in post-IMS mode and a surface-induced dissociation (SID) or IMS-TOF-MS (Synapt G2S, Waters Corp.). The mass range was set to *m/z* 50 – 4000 with a 1 s scanning rate. The quadrupole profile was set automatically. The essential parameters of the mass spectrometer operating in "V-mode" were: 1 – 2 kV capillary voltage, 20 V sampling cone, 20 V source offset, 25 °C source temperature, 10 V trap collision energy, 10 V transfer collision energy, 5 – 20 mL/min trap gas flow. A solution of a 20 mM cesium iodide (99.999%, analytical standard for HR-MS, Fluka) in a 50:50 acetonitrile:water was used as a calibration solution for the MS system. As an internal standard, $d(T)_6$ of 2.5 mM was added.

Thermal Denaturation MS

We used a laboratory-built temperature-controlled nanoelectrospray (TC-nESI) source first introduced by Marchand et al.[5] Borosilicate nanoelectrospray emitters of ~1 µm I.D. (B-100-75-10, Sutter Instrument) were made using micropipette puller equipped with metal filament (P1000, Sutter Instrument). The ESI emitter, filled with 5 – 10 µL of oligonucleotide solution, is placed between two temperature-controlled copper blocks that guarantee uniform heat distribution. The ESI emitter tip protruded from the copper blocks towards the MS inlet by no more than 1 mm. A Peltier element was used to precisely control the temperature of the copper parts, emitter and the sample solution, in the range of 13 – 90 °C. For thermal denaturation MS experiments, the rate of temperature increase was set to 1 °C/min, to minimize the appearance of kinetic products of DNA melting.[64] More details on data processing are given in Supporting Information.

Results and Discussion

Previous studies have indicated that non-covalent DNA complexes can be preserved in the gas phase.[38,39] Therefore, it is possible to use TC-nESI to interrogate the structural aspects which contribute to the stability of a oligonucleotides complex.[5,59] Other TC-nESI studies have focused on duplexes and quadruplexes. However, none of these studies have dealt with more complicated structures, let alone the unfolding and dissociation pathways of TWJs, nor was ion mobility spectrometry (IMS) used to examine the effects of heating on oligonucleotide conformational states. Also, there is a distinct lack of studies that focus on comparing gas-phase with solution stabilities. The focus of this work is to address these issues for TWJs.

Identification of Intermediates

For the initial melting experiments, two TWJs called TWJ-1 and TWJ-2 were tested to ascertain that structural information could indeed be obtained from such melting experiments. Duplex intermediates generated from melting this TWJ-1 had the potential to form different conformational states due to binding of mismatched base pairs. The mass spectra extracted at specific temperatures from the melting experiments showed multiple charge state series varying with the molecular mass of oligonucleotides (Figure 1B). For TWJ-1, the peaks for single strands were observed from *m/z* 1200 to 1700, for dimers from *m/z* 1500 to 2000, and for the intact TWJ from *m/z* 1600 to 2500 (Figure 1B and S1). To generate the melting curves, the peak areas for each charge state were extracted and plotted as a function of temperature. (Figure 2A).

These data showed that, as temperature increased, both TWJ-1 and TWJ-2 dissociated into duplex intermediates and then to monomers. TWJ-1 had a typical sigmoidal melting curve, with T_m = 45 ± 1 °C. Between 35 and 70 °C, the charge state distributions corresponding to all three possible duplex-like intermediates (*1:2*, *1:3*, and *2:3*) were observed at T_{max} of ~50 °C (T_{max} is defined as a temperature where the species reaches the highest abundance). The MS melting of TWJ-1 and TWJ-2 revealed minor differences in thermal stabilities of the duplex-like intermediates (Figure 2B and S2, respectively). Specifically, the T_{max} for the *2:3* complex is shifted by 3 °C to lower temperature compared to the other intermediates. The UV-melting experiments, performed under the same solvent conditions as the MS melting experiments, showed an ambiguous, two-step dissociation (Figure S3). This variation in thermostability was also evident when comparing with the MS melting of individual duplexes (Figure S4), where the T_m of the *2:3* complex was found to be significantly higher (by 6 – 8 °C) compared to two other duplexes. In contrast, the MS melting temperature matches the first step inflection point, which indicated T_m = 47.7 °C. This implies that the *2:3* duplex, with the highest number of additional base pairs (bps), is more stable than the other two duplexes and competes with TWJ formation. The van't Hoff analysis showed the difference of $\Delta G°$ = 6.7 kJ/mol (Figure S9). Based on this information, we propose that the potential differences in T_{max} values originate from the additional bps forming in the overhanging sequences of intermediate

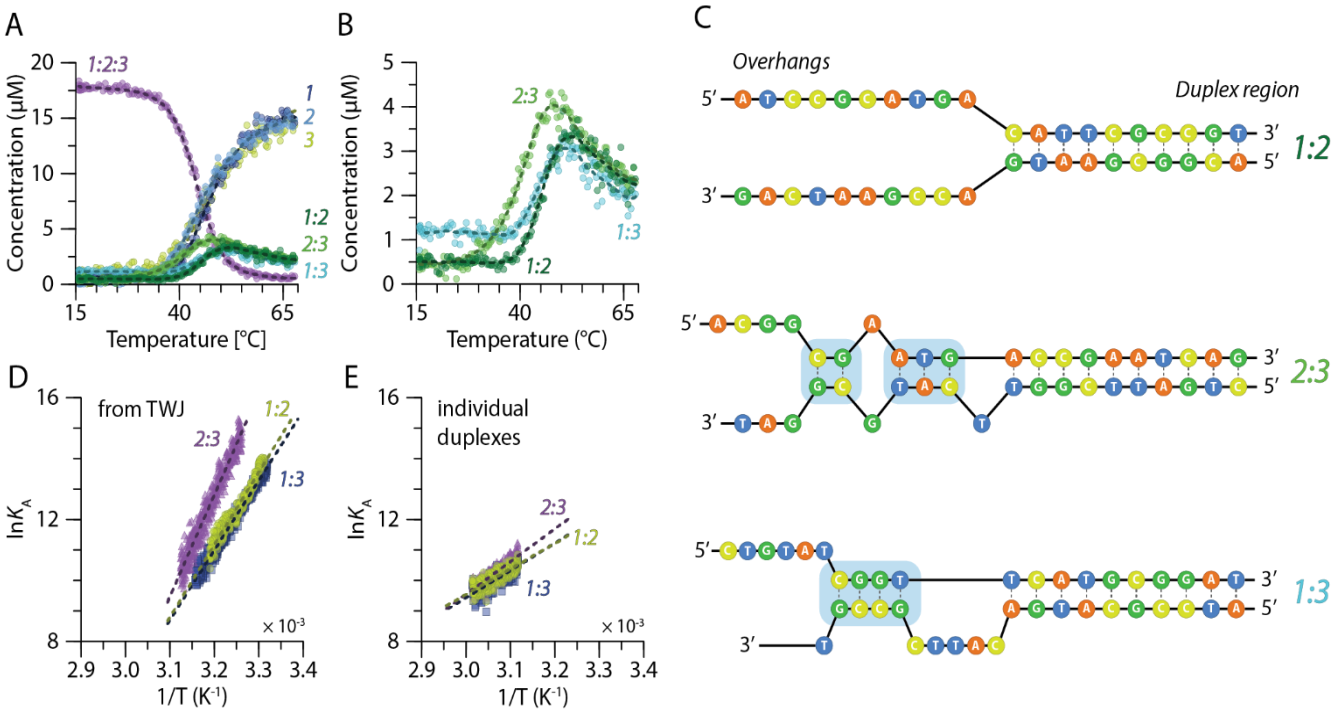

Figure 2: Thermal characterization of the TWJ-1 complex composed of 10 bps in each arm in 100 mM ammonium acetate. (A) The MS thermal denaturation profiles of 20 μM (each strand) TWJ-1 with (B) magnified view of duplex-like intermediates, (fit: LOWESS). (C) Putative structures of the duplex-like intermediates according to 'DINAMelt Server' structural simulation; formation of additional base pairs between overhanging strands highlighted in light blue. The ion concentrations, crucial for comparison with the MS thermal denaturation experiments, were set to 20 μM (each strand), 100 mM (Na^+), and 0 mM (Mg^{2+}) (D) Comparison of Van't Hoff analyses of duplex-like intermediates formed from TWJ-3 and (E) of individual duplexes in the absence of the corresponding third strand.

duplexes. To test this hypothesis, a nearest-neighbor analysis of duplexes (DINAMelt)[65] was performed to identify the formation of the bps in the overhangs (Figure 2C).[63,66] The simulation of the *1:2* complex showed no additional base-pairing between the overhangs. In contrast, three additional C≡G bps and one non-canonical T=G pair[67] were predicted to occur in the overhangs of the *1:3* complex. These simulations suggest that the energy difference is due to the large 5-nt bulge in strand 3 and the remaining overhang of strand 1. Melting curves were also simulated and plotted as a function of temperature (Figure S5). This revealed another phenomenon that could be a potential source of thermodynamic inconsistencies between simulation, gas-phase or solution-phase analysis: long single-stranded oligonucleotides are prone to form hairpins or self-dimers. The *2:3* complex was predicted to form a hairpin-like intermediate formed by strand 2, reaching almost 50% abundance during the simulated melting. This additional interaction may significantly alter the TWJ stability. By mixing only two of the TWJ-forming strands, we could compare the T_m values of duplex-like intermediates with those that do not originate from the TWJ. Both MS- and UV-melting experiments (Figure S4 and S6) identified a significant stabilization within the *2:3* duplex, with a T_m increase of 6–8 °C and a ΔG_A° decrease of −8 kJ/mol, which is contrary to the simulations. Experimental data can differ from simulations due to differences in ionic strength, ion type, or in the concentrations used. Discrepancies may also arise from the noise in the mass spectra, especially when considering low-abundance signals. Lower T_m values were observed for all duplex-forming systems when one of the three strands was not present in the mixture.

DNA melting can be a complex process involving partially melted intermediates comprising both double-stranded and melted regions. While photometric or calorimetric methods measure T_m as the dissociation of 50% base pairs, MS measurements provide T_m that can be defined as 50% dsDNA molecules being fully dissociated into two ssDNA. To distinguish between these two definitions of T_m, IMS measurements were conducted. TC-ESI-IMS-MS experiments on TWJ-1 and TWJ-2 showed minimal or negligible changes in arrival time distribution (ATD), as depicted in Figures S7 and S8. Such changes in ATD have been demonstrated to give evidence about changes in the conformation of DNA complexes.[68] This implies that, despite the anticipated zipper-like opening, we observed dissociation of full dsDNA regions as a single-step process. Although significant differences in thermodynamic data obtained from MS melting were observed and could be caused by additional base pair formation/breakage, such interactions do not substantially alter the TWJ secondary structure and its dissociation intermediates in the gas phase.

The van't Hoff analysis of MS melting showed a significant difference in ΔG_A° of duplexes released from individual duplexes relative to the TWJ complex, with an average of −20 kJ/mol, as depicted in Figure 2D and 2E (details shown in Figure S9). Altogether, this could be interpreted as the stability of TWJ being higher than the stability of any individual duplexes. This thermodynamic property of TWJ makes it a promising candidate for use as a specific and reliable probe for detecting single-stranded oligonucleotides[15] and influencing the stability of branchpoints *in vivo*.[69]

Effect of GC Base-Pairing on TWJ Dissociation

The stability of DNA is significantly influenced by its nucleotide composition. This is because GC bps (with three hydrogen bonds) provide a stronger stabilizing effect compared to AT pairs (with only two hydrogen bonds). To investigate the effect of strand composition on the TWJ dissociation pathway, we designed TWJ-3 without mismatches or bulges in the overhangs. The TWJ-3 structure was designed to contain two, four, or six GC bps in each 8-bp-long arm (Table 1). An overview mass spectrum with the main TWJ-3 forms is shown in Figure 1B. Using TC-nESI-MS, the relative abundances of TWJ-3 forms were obtained and plotted as a function of temperature (Figure 3). Starting with fully formed TWJ-3, we observed a significant increase in the abundance of duplex-like intermediates depending on the number of GC bps in the original TWJ-3. A study of the intermediate melting curves showed significant variation in their gradients when the temperatures rose above 30 °C. The least stable intermediate, i.e., the *1:2* duplex, was detected at an insignificant level during the entire temperature ramp; its low stability is mainly caused by the presence of only two GC bps involved in binding. Supporting this, UV-melting of individual duplexes did not show a sigmoidal melting curve for the *1:2* complex (Figure S10), which suggests the absence of any folded duplex at the starting temperature. With a higher number of GC bps, we observed a steeper gradient for the *1:3* and, more notably, for the *2:3* complex. These species reach a maximum abundance at a solution temperature between 40 and 45 °C. Interestingly, the melting profiles of individual strands appear to rise with two different slopes. At temperatures below 45 °C, we first observed dissociation of the TWJ-3 into duplexes and monomers. The change of the main source of monomers (see Figure 3) is identified around 45 °C, where a change in the monomer curve slopes could be identified corresponding with the T_{max} of duplex intermediates (indicated by dashed line in the Figure 3). The complex melting profiles are the reason why the melting temperatures could not be directly obtained from the melting

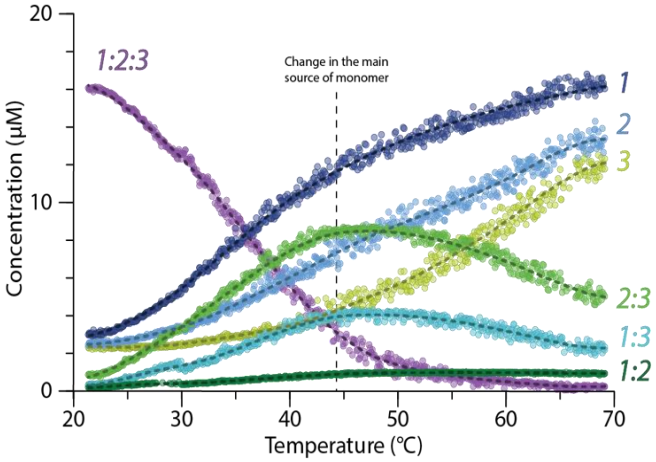

Figure 3: MS thermal analysis of the 20 µM TWJ-3 composed of 8 bps in each arm using TC-nESI-MS, (fit: LOWESS). MS thermal denaturation profiles extracted from MS data, temperature gradient of 1 °C/min. A change in the dissociation process is indicated with a dashed line (see text). Dissociation of the *1:2:3* complex results in three duplex-like intermediates (left) followed by dissociation of the generated duplex-like intermediates into single strands (right).

curves. Instead, the T_m values were calculated from the thermodynamic data (Figure S11), which showed 28.1 ± 1.1 °C for two GC bps (*1:2*), 33.9 ± 1.7 °C for four GC bps (*1:3*), and 47.4 ± 2.9 °C for six GC bps (*2:3*). The overall stabilizing trend showed a decrease in ΔG_A° by 3 kJ/mol per every 2 additional GC bps. Simultaneously, the TWJ-3 abundance reaches an insignificant level. Instead, the still-folded *1:3* and *2:3* duplexes become the main sources of monomers. The differences in intermediate stabilities suggest a delicate balance of the forces involved in the TWJ formation with the main contribution of number bps in each arm. The results suggest a complex dissociation mechanism with multiple pathways as proposed in Figure 1.

Effect of Ligand Binding

A cavity in the center of TWJs may act as a specific binding site for small molecules. Two previously reported TWJ-binding drugs with high specificity, azacryptands 2,7-TrisNP (hereafter TrisNP) and TrisPOB, were investigated in this study (mass spectra in Figure S12, structures in Figure S13).[24,70,71] The binding and stabilizing effect of these drugs on the TWJ-3 were measured by UV melting, CD, TC-nESI-MS, and SID. The CD spectra showed spectral changes upon ligand binding in the range of 210 – 320 nm (Figure S14) in agreement with previous literature.[35] Changes in this range can be attributed to several phenomena, such as binding of ligands in the chiral TWJ cavity site[28,72] or when the TWJ structure changes between different conformations.[73]

The UV-melting experiment showed an ambiguous melting profile of TWJ-3, suggestive of two-step dissociation. However, in the presence of TrisNP or TrisPOB, we observed a sigmoidal, single-step melting curves with T_m values of 52 and 55 °C, respectively (Figure 4A). Consistent with UV-melting experiments, a significant increase of T_m of TWJ-3 in the presence of ligands was observed using TC-nESI-MS (Figure 4B). When 7 µM of TWJ-3 were mixed with an equivalent amount of TrisNP or TrisPOB, the T_m increased from 31.9 to 45.0 or 58.0 °C, respectively. The melting curves of intermediates showed their significant stabilization. Even at 90 °C, i.e., the upper temperature limit of the TC-nESI source, we could not detect any dissociation of duplex-like intermediates when the ligand was added to the TWJ. Notably, in the presence of TrisNP, we could identify the presence of free TWJ-3 with a maximum abundance of 40% at 52 °C. In contrast, free TWJ-3 was not detected at any significant abundance when TrisPOB was added. We hypothesize that TrisPOB binding raises the T_m of TWJ-3 to the point where it outweighs the stability of TWJ; as a result, simultaneous dissociation of all TWJ were observed. Furthermore, this observation highlights the fine differences in the ligand-induced effects on TWJ dissociation that are not revealed by a simple comparison of T_m data obtained from UV-melting or CD experiments. Finally, when we compared MS melting of TWJ-3 alone and in the presence of TrisNP or TrisPOB, we found that the appearance of unfolding curves became cooperative, especially when TWJ-3 was mixed with TrisPOB. This suggests that ligand bound the central branchpoint cavity in 1:1 ratio and can prevent TWJ from sequential dissociation. This is also supported by low-abundant signals of duplex:ligand complexes in the mass spectra (Figure S12).

To corroborate this observation, we performed SID measurement on TWJ-3 in the absence or presence of ligands. To the best of our knowledge, this is the first time that SID is applied to multimeric DNA complexes. SID employs the impact of biomolecules on an electrode surface leading to the release of individual complex subunits. Compared to other gas-phase fragmentation techniques like collision-induced dissociation (CID) or electron-capture dissociation (ECD), SID is exclusively capable of providing insights into the secondary structure and stability of biomolecular complexes in the gas phase.

Unlike for peptides and proteins,[73,74] the SID mass spectra showed considerable fragmentation (Figure S15). However, as demonstrated in Figure 4C, all single strands appeared with similar profiles in the presence of ligands. The SID energy required to unfold 50% of the TWJ-3 was found to be 38 V. Matching the UV-melting and TC-nESI-MS experiments, higher energies (41 and 43 V, respectively) were required for complexes with TrisNP and TrisPOB.

These findings suggest a comparable stabilizing effect in the gas phase upon ligand binding as shown by the TC-nESI-MS experiments. However, intermediate profiles vary between solution and gas-phase melting/unfolding. Ionic strength and solvation of polyanionic DNA backbone are known to have a tremendous effect on the stability and the structure of oligonucleotide complexes.[41,47,48] In the gas phase, we expect high electrostatic repulsions altering the structures and ligand binding. Solution and gas-phase results have shown increasing energy required for melting of the TWJ upon ligand binding. However, the differences between intermediates stability and their affinity towards the ligands are changed in the gas phase. Altogether, Figure 4 illustrates the complexity associated with formation of the TWJ and its binding to the specific TWJ-binding ligands.

Conclusions

In conclusion, this study provides valuable insights into the thermodynamics and dissociation mechanisms of three TWJs in both solution and gas phase using a combination of TC-nESI-MS, SID, UV-melting, and CD spectroscopy. The ability to differentiate and quantify various distinct solution and gas-phase populations and intermediates at different temperatures provides detailed information about the TWJ species involved in complex dissociation. Collectively, our results suggest that the melting process of TWJs proceeds in a stepwise, multi-pathway fashion in the absence of ligands, but becomes more uniform in the presence of TWJ-binding ligands. The examination of IMS data demonstrated that neither the TWJ complexes nor the duplex-like intermediates exhibited any change in drift time during the temperature ramp. This observation suggests that the release of the DNA strand is a single-step process. These findings highlight the

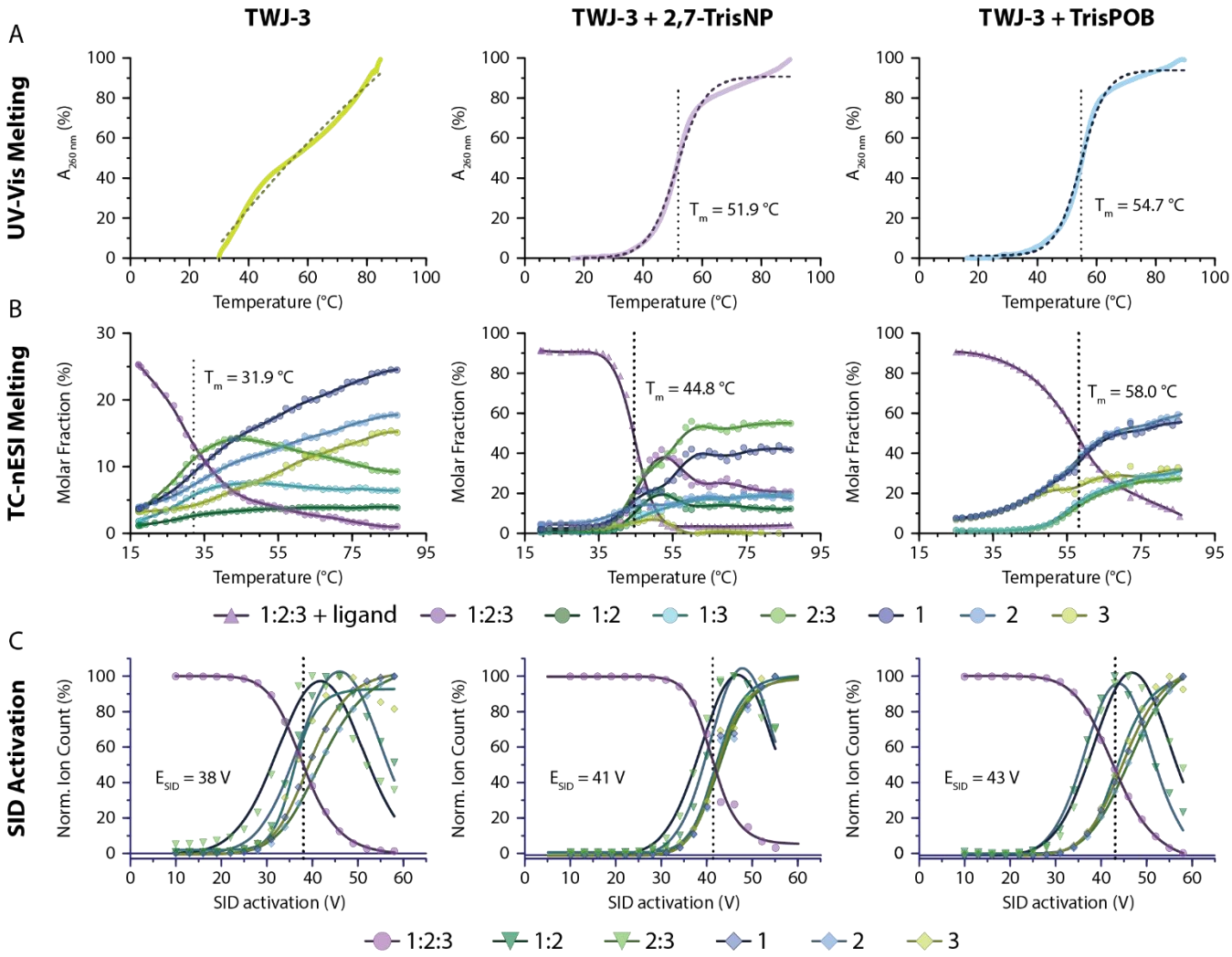

Figure 4: Effect of TWJ-binding ligands on dissociation of 7 µM TWJ-3 complex in 100 mM AmAc. (A) UV-Vis thermal denaturation profiles, fit: sigmoidal, 4PL of 7 µM TWJ-3 in the absence and in the presence of ligands, temp. gradient of 0.2 °C/min. (B) The TC-nESI-MS thermal denaturation profiles of 7 µM TWJ-3 without ligand (left), with 7 µM TrisNP (center) or 7 µM TrisPOB (right), temp. gradient of 1 °C/min, fit: LOWESS. (C) Profiles showing normalized intensity of individual species as a function of SID voltage, energy gradient of 3V/step, fit: sigmoidal, 4PL or Gaussian. T_m/E_{SID} is shown as a dashed line.

importance of considering the effects of parameters such as strand length, composition, and ligands in future applications of DNA/RNA branchpoints. These parameters are important to consider when developing applications of diagnostic tools based on oligonucleotide structures. The methodology presented here can be used for the detailed characterization of TWJ aptamers from systematic evolution of ligands by exponential enrichment (SELEX) to investigate unfolding in the absence and presence of ligands (e.g., MN4 aptamer) or oligonucleotide-based sensing systems. Here, we have shown that state-of-the-art TC-nESI-MS, combined with SID and IMS, are valuable analytical techniques that can support standard solution-based methods and provide detailed information on dissociation mechanism and energetics of binding events. A combined methodology based on MS and other techniques can provide fast and precise information for developing of DNA structural probes,[15,17] nano-architectures,[75] aptamers,[76] and biomolecular diagnostic tools.[77]

ASSOCIATED CONTENT

Supporting Information

The Supporting Information is available free of charge on the ACS Publications website. Mass spectrum of TWJ-1 (Figure S1); MS-melting of TWJ-2 (Figure S2); UV-melting of TWJ-1 (Figure S3); MS melting of individual TWJ-1 duplexes (Figure S4); Simulated melting profiles of TWJ-1 duplexes showing internal folding (Figure S5); UV-melting profiles of TWJ-1 duplexes (Figure S6); Heat maps of individual TWJ-1 forms (Figure S7); Heat maps of individual TWJ-2 forms (Figure S8); Thermodynamic comparison of TWJ-1 (Figure S9); UV-melting profile of TWJ-3 (Figure S10); Van't Hoff plot of TWJ-3 (Figure S11); Mass spectra of TWJ-3 with ligands (Figure S12); Structures of used ligands (Figure S13); The CD spectra of TWJ-3 with ligands (Figure S14); SID spectra of TWJ-3 mixed with ligands at different SID energies (Figure S15). The original date are available in an ETH Zurich data archive (www.research-collection.ethz.ch) under the doi 10.3929/ethz-b-000574178.

AUTHOR INFORMATION

Corresponding Author

Renato Zenobi – Department of Chemistry and Applied Biosciences, ETH Zurich, CH-8093 Zurich, Switzerland; orcid.org/0000-0001-5211-4358; Phone: +41 44 632 43 76; Email: zenobi@org.chem.ethz.ch; Fax: +41 44 632 292

Authors

Adam Pruška‡ – Department of Chemistry and Applied Biosciences, ETH Zurich, CH-8093 Zurich, Switzerland

Julian A. Harrison‡ – Department of Chemistry and Applied Biosciences, ETH Zurich, CH-8093 Zurich, Switzerland

Adrien Marchand – Department of Chemistry and Applied Biosciences, ETH Zurich, CH-8093 Zurich, Switzerland

Anton Granzhan – CNRS UMR9187, Inserm U1196, Institut Curie, Paris Saclay University, F-91405 Orsay, France

ACKNOWLEDGMENTS

Circular dichroism and UV data were collected with the help of V. Islami (group of Prof. H. Wennemers) and with help of T. Murnauer (group of Prof. K. Lang) from ETH Zurich. We thank Dr. D. Monchaud (University of Burgundy) for stimulating discussions and all members of the Zenobi group, particularly P. Bittner. We thank the Swiss National Science Foundation (grant no. 200020_207354) and French National Research Agency (grant no. ANR-22-CE44-0039) for financial support of this work. There are no conflicts of interest to declare.

REFERENCES

1. Lilley, D. M. J. Structures of Helical Junctions in Nucleic Acids. *Q. Rev. Biophys.* **2000**, *33* (2), 109–159.
2. Chou, S. H.; Chin, K. H.; Wang, A. H. J. Unusual DNA Duplex and Hairpin Motifs. *Nucleic Acids Res.* **2003**, *31* (10), 2461–2474.
3. Haider, S. Computational Methods to Study G-Quadruplex–Ligand Complexes. *J. Indian Inst. Sci.* **2018**, *98* (3), 325–339.
4. O. Tucker, W.; T. Shum, K.; A. Tanner, J. G-Quadruplex DNA Aptamers and Their Ligands: Structure, Function and Application. *Curr. Pharm. Des.* **2012**, *18* (14), 2014–2026.
5. Marchand, A.; Rosu, F.; Zenobi, R.; Gabelica, V. Thermal Denaturation of DNA G-Quadruplexes and Their Complexes with Ligands: Thermodynamic Analysis of the Multiple States Revealed by Mass Spectrometry. *J. Am. Chem. Soc.* **2018**, *140* (39), 12553–12565.
6. Campbell, N.; Collie, G. W.; Neidle, S. Crystallography of DNA and RNA G-Quadruplex Nucleic Acids and Their Ligand Complexes. *Curr. Protoc. Nucleic Acid Chem.* **2012**, *50* (SUPLL.50), 17.6.1-17.6.22.
7. Winnerdy, F. R.; Das, P.; Heddi, B.; Phan, A. T. Solution Structures of a G-Quadruplex Bound to Linear- A Nd Cyclic-Dinucleotides. *J. Am. Chem. Soc.* **2019**, *141* (45), 18038–18047.
8. Assi, H. A.; Garavís, M.; González, C.; Damha, M. J. I-Motif DNA: Structural Features and Significance to Cell Biology. *Nucleic Acids Res.* **2018**, *46* (16), 8038–8056.
9. Khristenko, N.; Amato, J.; Livet, S.; Pagano, B.; Randazzo, A.; Gabelica, V. Native Ion Mobility Mass Spectrometry: When Gas-Phase Ion Structures Depend on the Electrospray Charging Process. *J. Am. Soc. Mass Spectrom.* **2019**, *30* (6), 1069–1081.
10. Ciccia, A.; Elledge, S. J. The DNA Damage Response: Making It Safe to Play with Knives. *Mol. Cell* **2010**, *40* (2), 179–204.
11. Dobbelstein, M.; Sørensen, C. S. Exploiting Replicative Stress to Treat Cancer. *Nat. Rev. Drug Discov.* **2015**, *14* (6), 405–423.
12. Zell, J.; Sperti, F. R.; Britton, S.; Monchaud, D. DNA Folds Threaten Genetic Stability and Can Be Leveraged for Chemotherapy. *RSC Chem. Biol.* **2021**, *2* (1), 47–76.
13. Peng, Z.; Liu, H. Bottom-up Nanofabrication Using DNA Nanostructures. *Chem. Mater.* **2016**, *28* (4), 1012–1021.
14. Saraswathi, S. K.; Vittala, S. K.; Manayani, M. K.; Joseph, J. Sequence Programmed DNA Three-Way Junctions for Templated Assembly of Fluorescent Silver Nanoclusters. *J. Photochem. Photobiol. B Biol.* **2020**, *207*, 111886.
15. Zhang, H.; Li, X.; He, F.; Zhao, M.; Ling, L. Turn-off Colorimetric Sensor for Sequence-Specific Recognition of Single-Stranded DNA Based upon Y-Shaped DNA Structure. *Sci. Rep.* **2018**, *8* (1), 12021.
16. Li, F.; Lin, Y.; Le, X. C. Binding-Induced Formation of DNA Three-Way Junctions and Its Application to Protein Detection and DNA Strand Displacement. *Anal. Chem.* **2013**, *85* (22), 10835–10841.
17. Van Riesen, A. J.; Le, J.; Slavkovic, S.; Churcher, Z. R.; Shoara, A. A.; Johnson, P. E.; Manderville, R. A. Visible Fluorescent Light-up Probe for DNA Three-Way Junctions Provides Host-Guest Biosensing Applications. *ACS Appl. Bio Mater.* **2021**, *4* (9), 6732–6741.
18. Xia, J.; Lin, M.; Zuo, X.; Su, S.; Wang, L.; Huang, W.; Fan, C.; Huang, Q. Metal Ion-Mediated Assembly of DNA Nanostructures for Cascade Fluorescence Resonance Energy Transfer-Based Fingerprint Analysis. *Anal. Chem.* **2014**, *86* (14), 7084–7087.
19. Roncancio, D.; Yu, H.; Xu, X.; Wu, S.; Liu, R.; Debord, J.; Lou, X.; Xiao, Y. A Label-Free Aptamer-Fluorophore Assembly for Rapid and Specific Detection of Cocaine in Biofluids. *Anal. Chem.* **2014**, *86* (22), 11100–11106.
20. Wang, X.; Seeman, N. C. Assembly and Characterization of 8-Arm and 12-Arm DNA Branched Junctions. *J. Am. Chem. Soc.* **2007**, *129* (26), 8169–8176.
21. Al-Shareef, W.; Brown, Y.; Bryan, C.; Shuvaeva, E.; Bsoul, S.; Greenman, R.; Kabaha, M. M.; Ulyanov, N. B.; Skordalakes, E.; Tzfati, Y. Functional Interactions of Kluyveromyces Lactis Telomerase Reverse Transcriptase with the Three-Way Junction and the Template Domains of Telomerase RNA. *Int. J. Mol. Sci.* **2022**, *23* (18), 10757.
22. Fouché, N.; Cesare, A. J.; Willcox, S.; Özgür, S.; Compton, S. A.; Griffith, J. D. The Basic Domain of TRF2 Directs Binding to DNA Junctions Irrespective of the Presence of TTAGGG Repeats. *J. Biol. Chem.* **2006**, *281* (49), 37486–37495.
23. Li, K.; Wang, L.; Xu, X.; Gao, T.; Yan, P.; Jiang, W. Protein Binding-Protected DNA Three-Way Junction-Mediated Rolling Circle Amplification for Sensitive and Specific Detection of Transcription Factors. *RSC Adv.* **2016**, *6* (73), 68846–68851.
24. Duskova, K.; Lamarche, J.; Amor, S.; Caron, C.; Queyriaux, N.; Gaschard, M.; Penouilh, M. J.; De Robillard, G.; Delmas, D.; Devillers, C. H.; Granzhan, A.; Teulade-Fichou, M. P.; Chavarot-Kerlidou, M.; Therrien, B.; Britton, S.; Monchaud, D. Identification of Three-Way DNA Junction Ligands through Screening of Chemical Libraries and Validation by Complementary in Vitro Assays. *J. Med. Chem.* **2019**, *62* (9), 4456–4466.
25. Guyon, L.; Pirrotta, M.; Duskova, K.; Granzhan, A.; Teulade-Fichou, M. P.; Monchaud, D. Twj-Screen: An Isothermal Screening Assay to Assess Ligand/DNA Junction Interactions in Vitro. *Nucleic Acids Res.* **2018**, *46* (3), e16.
26. Vuong, S.; Stefan, L.; Lejault, P.; Rousselin, Y.; Denat, F.; Monchaud, D. Identifying Three-Way DNA Junction-Specific Small-Molecules. *Biochimie* **2012**, *94* (2), 442–450.
27. Takezawa, Y.; Yoneda, S.; Duprey, J. L. H. A.; Nakama, T.; Shionoya, M. Metal-Responsive Structural Transformation between Artificial DNA Duplexes and Three-Way Junctions. *Chem. Sci.* **2016**, *7* (5), 3006–3010.

28. McQuaid, K. T.; Pipier, A.; Cardin, C. J.; Monchaud, D. Interactions of Small Molecules with DNA Junctions. *Nucleic Acids Res.* **2022**, *50* (22), 12636–12656.
29. Phongtongpasuk, S.; Paulus, S.; Schnabl, J.; Sigel, R. K. O.; Spingler, B.; Hannon, M. J.; Freisinger, E. Binding of a Designed Anti-Cancer Drug to the Central Cavity of an RNA Three-Way Junction. *Angew. Chemie - Int. Ed.* **2013**, *52* (44), 11513–11516.
30. Yang, Z.; Chen, Y.; Li, G.; Tian, Z.; Zhao, L.; Wu, X.; Ma, Q.; Liu, M.; Yang, P. Supramolecular Recognition of Three Way Junction DNA by a Cationic Calix[3]Carbazole. *Chem. - A Eur. J.* **2018**, *24* (23), 6087–6093.
31. Ivens, E.; Cominetti, M. M. D.; Searcey, M. Junctions in DNA: Underexplored Targets for Therapeutic Intervention. *Bioorganic Med. Chem.* **2022**, *69*, 116897.
32. Zell, J.; Monchaud, D. Targeting DNA Junctions with Small Molecules for Therapeutic Applications in Oncology. *Handb. Chem. Biol. Nucleic Acids* **2022**, 1–24.
33. Kadrmas, J. L.; Ravin, A. J.; Leontis, N. B. Relative Stabilities of DNA Three-Way, Four-Way and Five-Way Junctions (Multi-Helix Junction Loops): Unpaired Nucleotides Can Be Stabilizing or Destabilizing. *Nucleic Acids Res.* **1995**, *23* (12), 2212–2222.
34. Diamond, J. M.; Turner, D. H.; Mathews, D. H. Thermodynamics of Three-Way Multibranch Loops in RNA. *Biochemistry* **2001**, *40* (23), 6971–6981.
35. Novotna, J.; Laguerre, A.; Granzhan, A.; Pirrotta, M.; Teulade-Fichou, M. P.; Monchaud, D. Cationic Azacryptands as Selective Three-Way DNA Junction Binding Agents. *Org. Biomol. Chem.* **2015**, *13* (1), 215–222.
36. Wu, B.; Girard, F.; van Buuren, B.; Schleucher, J.; Tessari, M.; Wijmenga, S. Global Structure of a DNA Three-Way Junction by Solution NMR: Towards Prediction of 3H Fold. *Nucleic Acids Res.* **2004**, *32* (10), 3228–3239.
37. Heuer, A.; Thomson, E.; Schmidt, C.; Berninghausen, O.; Becker, T.; Hurt, E.; Beckmann, R. Cryo-EM Structure of a Late Pre-40S Ribosomal Subunit from Saccharomyces Cerevisiae. *Elife* **2017**, *6*.
38. Rosu, F.; De Pauw, E.; Gabelica, V. Electrospray Mass Spectrometry to Study Drug-Nucleic Acids Interactions. *Biochimie* **2008**, *90* (7), 1074–1087.
39. Marchand, A.; Gabelica, V. Native Electrospray Mass Spectrometry of DNA G-Quadruplexes in Potassium Solution. *J. Am. Soc. Mass Spectrom.* **2014**, *25* (7), 1146–1154.
40. Nguyen, G. T. H.; Leung, W. Y.; Tran, T. N.; Wang, H.; Murray, V.; Donald, W. A. Mechanism for the Binding of Netropsin to Hairpin DNA Revealed Using Nanoscale Ion Emitters in Native Mass Spectrometry. *Anal. Chem.* **2020**, *92* (1), 1130–1137.
41. Vallejo, D. D.; Rojas Ramírez, C.; Parson, K. F.; Han, Y.; Gadkari, V. V.; Ruotolo, B. T. Mass Spectrometry Methods for Measuring Protein Stability. *Chem. Rev.* **2022**, *122* (8), 7690–7719.
42. Zhong, Y.; Han, L.; Ruotolo, B. T. Collisional and Coulombic Unfolding of Gas-Phase Proteins: High Correlation to Their Domain Structures in Solution. *Angew. Chemie* **2014**, *126* (35), 9363–9366.
43. Al-jabiry, A.; Palmer, M.; Langridge, J.; Bellamy-Carter, J.; Robinson, D.; Oldham, N. J. Combined Chemical Modification and Collision Induced Unfolding Using Native Ion Mobility-Mass Spectrometry Provides Insights into Protein Gas-Phase Structure. *Chem. - A Eur. J.* **2021**, *27* (55), 13783–13792.
44. McAlary, L.; Harrison, J. A.; Aquilina, J. A.; Fitzgerald, S. P.; Kelso, C.; Benesch, J. L. P.; Yerbury, J. J. Trajectory Taken by Dimeric Cu/Zn Superoxide Dismutase through the Protein Unfolding and Dissociation Landscape Is Modulated by Salt Bridge Formation. *Anal. Chem.* **2020**, *92* (2), 1702–1711.
45. Eschweiler, J. D.; Kerr, R.; Rabuck-Gibbons, J.; Ruotolo, B. T. Sizing up Protein-Ligand Complexes: The Rise of Structural Mass Spectrometry Approaches in the Pharmaceutical Sciences. *Annu. Rev. Anal. Chem.* **2017**, *10*, 25–44.
46. Pan, S.; Sun, X.; Lee, J. K. DNA Stability in the Gas Versus Solution Phases: A Systematic Study of Thirty-One Duplexes with Varying Length, Sequence, and Charge Level. *J. Am. Soc. Mass Spectrom.* **2006**, *17* (10), 1383–1395.
47. Rueda, M.; Kalko, S. G.; Luque, F. J.; Orozco, M. The Structure and Dynamics of DNA in the Gas Phase. *J. Am. Chem. Soc.* **2003**, *125* (26), 8007–8014.
48. Saikusa, K.; Kato, D.; Nagadoi, A.; Kurumizaka, H.; Akashi, S. Native Mass Spectrometry of Protein and DNA Complexes Prepared in Nonvolatile Buffers. *J. Am. Soc. Mass Spectrom.* **2020**, *31* (3), 711–718.
49. Largy, E.; König, A.; Ghosh, A.; Ghosh, D.; Benabou, S.; Rosu, F.; Gabelica, V. Mass Spectrometry of Nucleic Acid Noncovalent Complexes. *Chem. Rev.* **2022**, *122* (8), 7720–7839.
50. Cao, Y.; Qin, Y.; Bruist, M.; Gao, S.; Wang, B.; Wang, H.; Guo, X. Formation and Dissociation of the Interstrand I-Motif by the Sequences d(XnC4Ym) Monitored with Electrospray Ionization Mass Spectrometry. *J. Am. Soc. Mass Spectrom.* **2015**, *26* (6), 994–1003.
51. Raab, S. A.; El-Baba, T. J.; Woodall, D. W.; Liu, W.; Liu, Y.; Baird, Z.; Hales, D. A.; Laganowsky, A.; Russell, D. H.; Clemmer, D. E. Evidence for Many Unique Solution Structures for Chymotrypsin Inhibitor 2: A Thermodynamic Perspective Derived from vT-ESI-IMS-MS Measurements. *J. Am. Chem. Soc.* **2020**, *142* (41), 17372–17383.
52. Blanc, J. C. Y. L.; Beuchemin, D.; Siu, K. W. M.; Guevremont, R.; Berman, S. S. Thermal Denaturation of Some Proteins and Its Effect on Their Electrospray Mass Spectrat. *Org. Mass Spectrom.* **1991**, *26* (10), 831–839.
53. Zenobi, R.; Harrison, J. A.; Pruška, A.; Bittner, P.; Muck, A.; Cooper-Shepherd, D. A. Advancing Cyclic Ion Mobility Mass Spectrometry Methods for Studying Biomolecules: Toward the Conformational Dynamics of Mega Dalton Protein Aggregates. *Anal. Chem.* **2022**, *94* (36), 12435–12443.
54. Köhler, M.; Marchand, A.; Hentzen, N. B.; Egli, J.; Begley, A. I.; Wennemers, H.; Zenobi, R. Temperature-Controlled Electrospray Ionization Mass Spectrometry as a Tool to Study Collagen Homo- and Heterotrimers. *Chem. Sci.* **2019**, *10* (42), 9829–9835.
55. Woodall, D. W.; El-Baba, T. J.; Fuller, D. R.; Liu, W.; Brown, C. J.; Laganowsky, A.; Russell, D. H.; Clemmer, D. E. Variable-Temperature ESI-IMS-MS Analysis of Myohemerythrin Reveals Ligand Losses, Unfolding, and a Non-Native Disulfide Bond. *Anal. Chem.* **2019**, *91* (10), 6808–6814.
56. Vermeer, A. W. P.; Norde, W. The Thermal Stability of Immunoglobulin: Unfolding and Aggregation of a Multi-Domain Protein. *Biophys. J.* **2000**, *78* (1), 394–404.
57. Benesch, J. L. P.; Sobott, F.; Robinson, C. V. Thermal Dissociation of Multimeric Protein Complexes by Using Nanoelectrospray Mass Spectrometry. *Anal. Chem.* **2003**, *75* (10), 2208–2214.
58. Hagen, T.; Laski, A.; Brümmer, A.; Pruška, A.; Schlösser, V.; Cléry, A.; Allain, F. H.-T.; Zenobi, R.; Bergmann, S.; Hall, J. Inosine Substitutions in RNA Activate Latent G-Quadruplexes. *J. Am. Chem. Soc.* **2021**, *143* (37), 15120–15130.
59. Pruška, A.; Marchand, A.; Zenobi, R. Novel Insight into Proximal DNA Domain Interactions from Temperature-Controlled Electrospray Ionization Mass Spectrometry. *Angew. Chemie - Int. Ed.* **2021**, *60* (28), 15390–15398.
60. Snyder, D. T.; Jones, B. J.; Lin, Y. F.; Cooper-Shepherd, D. A.; Hewitt, D.; Wildgoose, J.; Brown, J. M.; Langridge, J. I.; Wysocki, V. H. Surface-Induced Dissociation of Protein Complexes on a Cyclic Ion Mobility Spectrometer. *Analyst* **2021**, *146* (22), 6861–6873.
61. Giles, K.; Ujma, J.; Wildgoose, J.; Pringle, S.; Richardson, K.; Langridge, D.; Green, M. A Cyclic Ion Mobility-Mass Spectrometry System. *Anal. Chem.* **2019**, *91* (13), 8564–8573.
62. Harrison, J. A.; Pruška, A.; Oganesyan, I.; Bittner, P.; Zenobi, R. Temperature-Controlled Electrospray Ionization: Recent Progress and Applications. *Chem. - A Eur. J.* **2021**, *27* (72), 18015–18028.
63. Zuker, M. Mfold Web Server for Nucleic Acid Folding and Hybridization Prediction. *Nucleic Acids Res.* **2003**, *31* (13), 3406–3415.

64. Marchand, A.; Czar, M. F.; Eggel, E. N.; Kaeslin, J.; Zenobi, R. Studying Biomolecular Folding and Binding Using Temperature-Jump Mass Spectrometry. *Nat. Commun.* **2020**, *11* (1), 1–12.
65. Markham, N. R.; Zuker, M. DINAMelt Web Server for Nucleic Acid Melting Prediction. *Nucleic Acids Res.* **2005**, *33* (SUPPL. 2), W577–W581.
66. SantaLucia, J. A Unified View of Polymer, Dumbbell, and Oligonucleotide DNA Nearest-Neighbor Thermodynamics. *Proc. Natl. Acad. Sci. U. S. A.* **1998**, *95* (4), 1460–1465.
67. Ho, P. S.; Frederick, C. A.; Quigley, G. J.; van der Marel, G. A.; van Boom, J. H.; Wang, A. H.; Rich, A. G.T Wobble Base-Pairing in Z-DNA at 1.0 A Atomic Resolution: The Crystal Structure of d(CGCGTG). *EMBO J.* **1985**, *4* (13 A), 3617–3623.
68. Gabelica, V.; Baker, E. S.; Teulade-Fichou, M. P.; De Pauw, E.; Bowers, M. T. Stabilization and Structure of Telomeric and C-Myc Region Intramolecular G-Quadruplexes: The Role of Central Cations and Small Planar Ligands. *J. Am. Chem. Soc.* **2007**, *129* (4), 895–904.
69. Shu, D.; Shu, Y.; Haque, F.; Abdelmawla, S.; Guo, P. Thermodynamically Stable RNA Three-Way Junction for Constructing Multifunctional Nanoparticles for Delivery of Therapeutics. *Nat. Nanotechnol.* **2011**, *6* (10), 658–667.
70. Zell, J.; Duskova, K.; Chouh, L.; Bossaert, M.; Chéron, N.; Granzhan, A.; Britton, S.; Monchaud, D. Dual Targeting of Higher-Order DNA Structures by Azacryptands Induces DNA Junction-Mediated DNA Damage in Cancer Cells. *Nucleic Acids Res.* **2021**, *49* (18), 10275–10288.
71. Duskova, K.; Lejault, P.; Benchimol, É.; Guillot, R.; Britton, S.; Granzhan, A.; Monchaud, D. DNA Junction Ligands Trigger DNA Damage and Are Synthetic Lethal with DNA Repair Inhibitors in Cancer Cells. *J. Am. Chem. Soc.* **2020**, *142* (1), 424–435.
72. Heydari, M.; Moghadam, M. E.; Tarlani, A. A.; Farhangian, H. DNA as a Target for Anticancer Phen-Imidazole Pd(II) Complexes. *Appl. Biochem. Biotechnol.* **2017**, *182* (1), 110–127.
73. Carr, C. E.; Marky, L. A. Investigation of the Melting Behavior of DNA Three-Way Junctions in the Closed and Open States. *Biophys. J.* **2017**, *113* (3), 529–539.
74. Wysocki, V. H.; Joyce, K. E.; Jones, C. M.; Beardsley, R. L. Surface-Induced Dissociation of Small Molecules, Peptides, and Non-Covalent Protein Complexes. *J. Am. Soc. Mass Spectrom.* **2008**, *19* (2), 190–208.
75. Stiving, A. Q.; Vanaernum, Z. L.; Busch, F.; Harvey, S. R.; Sarni, S. H.; Wysocki, V. H. Surface-Induced Dissociation: An Effective Method for Characterization of Protein Quaternary Structure. *Anal. Chem.* **2019**, *91* (1), 190–209.
76. Wysocki, V. H.; Jones, C. M.; Galhena, A. S.; Blackwell, A. E. Surface-Induced Dissociation Shows Potential to Be More Informative Than Collision-Induced Dissociation for Structural Studies of Large Systems. *J. Am. Soc. Mass Spectrom.* **2008**, *19* (7), 903–913.
77. Hoon Roh, Y.; Ruiz, R. C. H.; Peng, S.; Lee, J. B.; Luo, D. Engineering DNA-Based Functional Materials. *Chem. Soc. Rev.* **2011**, *40* (12), 5730–5744.
78. Vörös, J.; Momotenko, D.; Nakatsuka, N.; Faillétaz, A.; Eggemann, D.; Forró, C. Aptamer Conformational Change Enables Serotonin Biosensing with Nanopipettes. *Anal. Chem.* **2021**, *93* (8), 4033–4041.
79. Wu, Y.; Belmonte, I.; Sykes, K. S.; Xiao, Y.; White, R. J. Perspective on the Future Role of Aptamers in Analytical Chemistry. *Analytical Chemistry*. 2019, pp 15335–15344.
80. Yu, J.; Liu, J.; Ma, C. B.; Qi, L.; Du, Y.; Hu, X.; Jiang, Y.; Zhou, M.; Wang, E. Signal-On Electrochemical Detection for Drug-Resistant Hepatitis B Virus Mutants through Three-Way Junction Transduction and Exonuclease III-Assisted Catalyzed Hairpin Assembly. *Anal. Chem.* **2022**, *94* (2), 600–605.
81. Moon, J.; Lim, J.; Lee, S.; Son, H. Y.; Rho, H. W.; Kim, H.; Kang, H.; Jeong, J.; Lim, E. K.; Jung, J.; Huh, Y. M.; Park, H. G.; Kang, T. Urinary Exosomal MRNA Detection Using Novel Isothermal Gene Amplification Method Based on Three-Way Junction. *Biosens. Bioelectron.* **2020**, *167*, 112474.